Scanning Microscopy

Volume 2 | Number 3 Article 3

6-4-1988

Application of Photovoltage Imaging to Semiconductor Wafer Characterization

Kanji Kinameri
Hitachi Ltd.

Chusuke Munakata
Hitachi Ltd.

Noriaki Honma
Hitachi Ltd.

Hiromichi Shimizu
Hitachi Ltd.

Follow this and additional works at: https://digitalcommons.usu.edu/microscopy

Part of the Biology Commons

Recommended Citation
Kinameri, Kanji; Munakata, Chusuke; Honma, Noriaki; and Shimizu, Hiromichi (1988) "Application of Photovoltage Imaging to Semiconductor Wafer Characterization," *Scanning Microscopy*: Vol. 2 : No. 3 , Article 3.
Available at: https://digitalcommons.usu.edu/microscopy/vol2/iss3/3

This Article is brought to you for free and open access by the Western Dairy Center at DigitalCommons@USU. It has been accepted for inclusion in Scanning Microscopy by an authorized administrator of DigitalCommons@USU. For more information, please contact digitalcommons@usu.edu.

Scanning Microscopy, Vol. 2, No. 3, 1988 (Pages 1237-1246)
Scanning Microscopy International, Chicago (AMF O'Hare), IL 60666 USA
0891-7035/88$3.00+.00

APPLICATION OF PHOTOVOLTAGE IMAGING TO SEMICONDUCTOR WAFER CHARACTERIZATION

Kanji Kinameri*, Chusuke Munakata, Noriaki Honma and Hiromichi Shimizu

Central Research Laboratory, Hitachi, Ltd., Kokubunji, Tokyo 185, Japan.

(Received for publication February 11, 1988, and in revised form June 04, 1988)

Abstract

A technique for imaging the distribution of ac surface photovoltages induced in a semiconductor wafer by the irradiation with a blue or near-infrared chopped photon beam is applied to non-destructive inspection of faults in Si or GaAs wafers. Faults detected include crystal defects, radiation damage, surface charge-up, striation and junction inhomogeneity. The principles of inspecting for the above mentioned wafer faults are quantitatively presented by numerical analyses of dependence of ac surface photovoltage on wafer electronic characteristics. The minimum detectable changes in minority carrier lifetime, interface trap density, fixed oxide charge density and resistivity for a depleted p-type Si wafer with a resistivity of 1Ωcm are estimated to be approximately 4%, 9%, 0.07% and 0.1%, respectively. For a weakly inverted wafer they are 4%, 250%, 1% and 4%, respectively. Examples of photovoltage images observed in Si wafers with swirl-like defects, grain boundaries, electron beam induced radiation damage, sulfate contamination and plasma induced surface charge up are shown together with images of an ion implanted GaAs wafer.

Key Words: surface photovoltage, flying spot scanner, semiconductor wafer, silicon, gallium arsenate, crystal defect, radiation damage, contamination, charge up, striation

*Address for Correspondence:
Central Research Laboratory, Hitachi, Ltd., Kokubunji, Tokyo 185, Japan.
Phone No.: 0423-23-1111, ext. 3411

Introduction

In semiconductor device fabrication it is very important to characterize wafers with regard to crystal defects, radiation damage, contamination, surface charge up and striation. These characterizations should be preferably non-destructive, but there are few techniques for non-destructive inspection of wafers. Crystal defects have been mapped using X-ray transmission topography (de Kock, 1973), EBIC (Czaja and Patel, 1965; Mataré and Laakso, 1968) and electron beam luminescence (Wittry and Kyser, 1964). With these techniques, however, wafers are damaged by radiation since the photon or electron energy is high enough to generate interface traps in the wafers.

To avoid the radiation damage, an optical beam induced current (OBIC) imaging method has frequently been applied to wafer characterizations by, e.g., Potter and Sawyer (1967), Haberer (1967), Saitoh et al (1976), Levy (1977) and Wilson et al (1979). In this method the distribution of dc OBIC (or simply photocurrent) is mapped. The OBIC imaging, however, cannot be applied to wafers at early stages of device fabrication, since ohmic contacts are indispensable to the wafers. Besides, radiation damage, contamination, surface charge up and striation can hardly be observed by OBIC imaging.

To facilitate non-destructive inspection for crystal defects and also for above surface/interface faults, a sophisticated method (Munakata et al, 1981) and apparatus (Kinameri et al, 1988) have been developed. In this method ac surface photovoltages (ac SPVs) induced in a semiconductor wafer by chopped photon irradiation are measured without any electrode contact with the wafer surface and are used as imaging signals. The present paper describes the principles of wafer characterization using this method and gives examples of its application to Si and GaAs wafers.

Photovoltage Imaging

Surface Photovoltage

In the oxide layer of an n-type Si wafer treated by an alkaline rinse or a thermally oxidized p-type Si wafer, charges with the same sign as majority carriers are fixed. Hence, a depletion layer with a strong electric field, e. g. $10^8 Vm^{-1}$, is formed beneath the oxide layer. A depletion layer is certain to be formed in a wafer with a p-n junction.

When such a wafer is irradiated by a photon beam (PB), surface photovoltage (SPV) (Brattain and Garrett, 1956) is induced across the depletion layer, because photocarriers excited in the wafer are separated by the depletion layer's electric field. Since SPV depends on electronic properties of the wafer (described later) the wafer can be characterized by SPV.

Apparatus

The apparatus for imaging SPV has been previously reported (Kinameri et al, 1988). It is basically a flying spot scanner as shown in Fig. 1. In Fig. 1, 2kHz ac SPVs induced in a specimen (wafer) by the irradiation of a chopped 0.4mm diameter PB are measured capacitively through a 25μm air gap between the wafer surface and a transparent electrode. Ac SPV distribution is obtained by scanning the photon beam on 512×480 points throughout a viewing field of 150×150mm maximum area. It is finally displayed on a TV monitor as a black and white image after electronic processing. Either a blue or near infrared PB can be chosen by switching cathode ray tubes to observe the surface and bulk of the wafer separately. The blue and near infrared PBs have 100μW maximum spot power peaking at 448nm and 10μW maximum spot power peaking at both 896nm and 1076nm, respectively. Measurement on a wafer is completed in about 5 minutes for a 512×480 pixel image, and about 1 minute for a 256×240 pixel image.

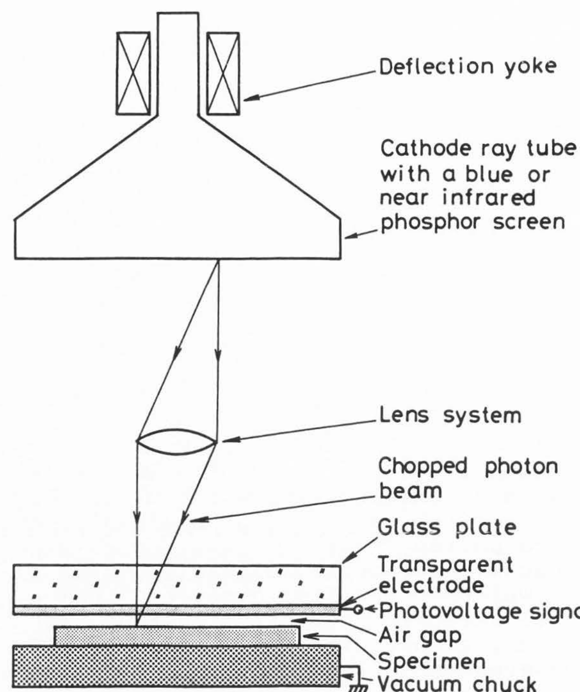

Fig. 1. Optical system for photovoltage imaging.

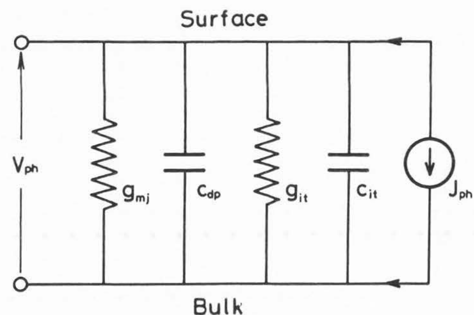

Fig. 2. Equivalent circuit for a depleted or weakly inverted p-type Si wafer (Munakata et al, 1986).

Principles of Wafer Characterizations

General

Electronic characteristics of a depleted or weakly inverted p-type Si wafer are represented by an equivalent circuit shown in Fig. 2 (Munakata and Nishimatsu, 1986). Ac SPV, V_{ph}, is thus expressed by

$$V_{ph} = J_{ph} z_{sf} , \quad (1)$$

where J_{ph} is PB induced photocurrent density, and z_{sf} is wafer surface impedance per unit area.

Apart from its dependence on PB power, J_{ph} is dominated by minority carrier lifetime, τ_n (or diffusion length, L_n) as,

$$J_{ph} = C \frac{\alpha(w+L_n)}{\alpha L_n+1} , \quad (2)$$

$$L_n = \sqrt{D_n \tau_n} , \quad (3)$$

where α is the optical absorption coefficient, w is the depletion layer width, D_n is the electron diffusion constant, and C is the constant. τ_n is shortened by, e. g., crystal defects in a wafer.

As shown in Fig. 2, z_{sf} consists of a majority carrier conductance, g_{mj}, a

depletion layer capacitance, c_{dp}, an interface trap conductance, g_{it}, and an interface trap capacitance, c_{it}. As shown in Fig. 3, these conductances and capacitances are dominated by interface trap density, D_{it}, fixed oxide charge density, Q_f, and resistivity, ρ, which depend on wafer faults. Although depletion layer conductance, g_{dp}, should sometimes be included in z_{sf} when the wafer is weakly inverted, it is neglected here since it is considerably smaller than g_{mj} or the susceptance due to c_{dp} for the wafer specifications described later. The faults can be inspected by imaging ac SPV. The application of OBIC imaging is, however, limited to inspections of faults which vary τ_n (or L_n) , e.g., crystal defects.

excitations, are shown in Fig. 4. Although ac SPV depends only slightly on τ_n when excited by the blue PB, it depends strongly on τ_n when excited by the near infrared PB. That is, when excited by the blue PB, photocarriers are mainly excited in the depletion layer, and most of the electrons and holes are separated without recombination via defects because of the strong electric field in the depletion layer. On the other hand, when excited by the near infrared PB, excess electrons are excited through the bulk because of the low optical absorption coefficient of Si in the near infrared wavelength range, and some of them are annihilated by recombinations via defects during their diffusion towards the surface.

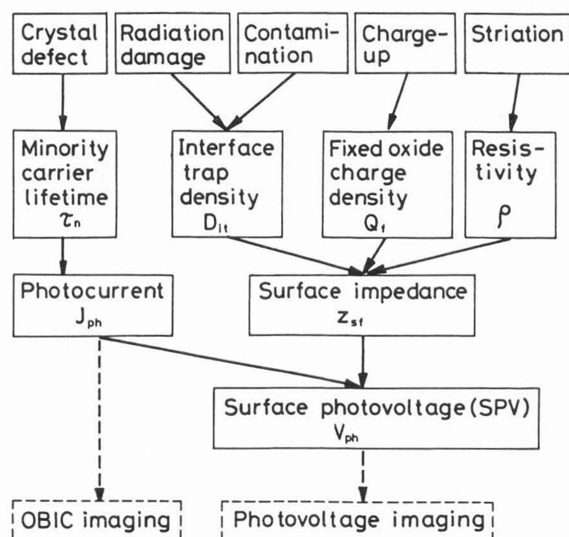

Fig. 3. Wafer faults detectable by photovoltage imaging.

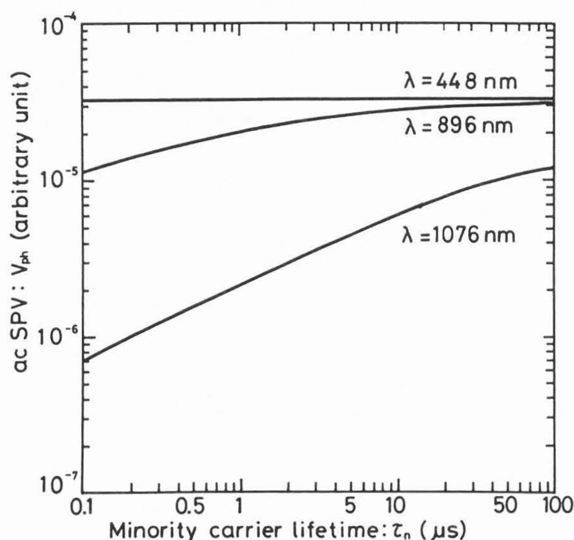

Fig. 4. Dependence of ac SPV on minority carrier lifetime.

Numerical Calculations

To confirm the applicability of the ac SPV imaging technique to wafer faults, dependence of 2kHz ac SPV on wafer characteristics such as τ_n, D_{it}, Q_f, and ρ, were calculated for a depleted or weakly inverted p-type Si wafer using the equations derived by Munakata et al (1984) and also by Munakata and Nishimatsu (1986). The standard wafer specifications for calculating ac SPVs are taken as τ_n=10μs, D_{it}=10^{14}m^{-2}eV^{-1}, Q_f=0.3mCm^{-2} and ρ=1Ωcm. The effects of wafer back surface were neglected.

Minority Carrier Lifetime

Dependence of ac SPV on minority carrier lifetime for a blue (448nm) and near infrared (896nm and 1076nm) PB

Interface Trap Density

Ac SPV dependence on interface trap density is shown in Fig. 5 for various fixed oxide charge densities. When Q_f=0.3mCm^{-2}, V_{ph} increases rapidly with D_{it}, but when Q_f=0.5mCm^{-2}, it decreases slightly. However, when Q_f=0.415mCm^{-2}, V_{ph} is almost independent of D_{it}. When Q_f=0.3mCm^{-2}, the wafer is depleted, i.e., the surface potential, ϕ_S, is lower than the Fermi potential, ϕ_F, and g_{mj} dominates z_{sf}. When Q_f=0.5mCm^{-2}, c_{dp} dominates z_{sf}, since the wafer is weakly inverted, i.e., ϕ_F<ϕ_S<$2\phi_F$. In a depleted wafer, vacant interface traps below the midgap level are additively (positively) charged to the fixed oxide charges. This increases ϕ_S, and significantly decreases g_{mj}. Accordingly, V_{ph} increases rapidly

with D_{it}. Conversely, the filled interface traps above the midgap level are charged subtractively (negatively) to the fixed oxide charges when the wafer is weakly inverted. This decreases ϕ_S and the depletion layer width, consequently increasing c_{dp}. Thus, V_{ph} decreases with an increase in D_{it}. When Q_f=0.415mCm^{-2}, ϕ_S is nearly equal to ϕ_F, and charges are trapped only a little at the interface. Since ϕ_S is thus kept almost constant, V_{ph} varies little in this particular case.

Such polarity inversions in interface trap charges have been demonstrated (Munakata et al, 1982) using the theoretical model by Iizuka and Sugano (1973), in which interface traps above and below the midgap level behave as acceptors and donors, respectively.

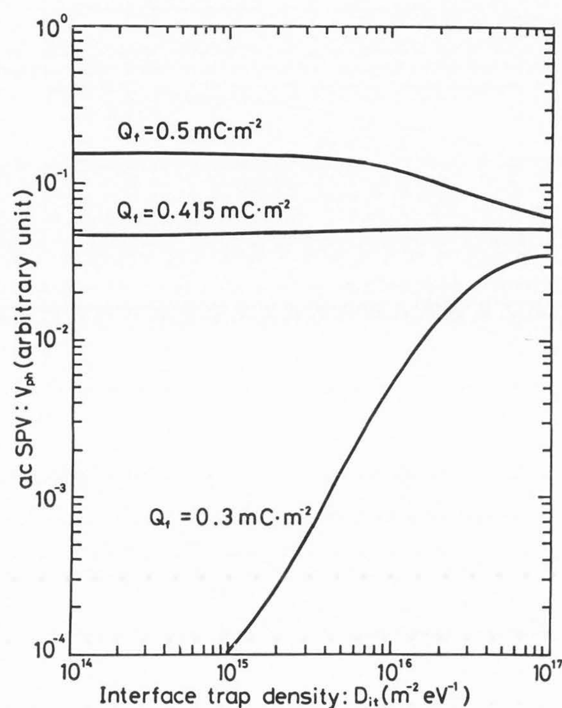

Fig. 5. Dependence of ac SPV on interface trap density.

Fixed Oxide Charge Density and Resistivity

Dependences of V_{ph} on fixed oxide charge density, Q_f, and resistivity, ρ, are shown in Figs. 6 and 7, respectively. As shown, V_{ph} always increases with both Q_f and ρ. The mechanisms of these dependences are similar to those for Fig. 5. Because an increase in ϕ_S with Q_f or ρ causes a decrease in both g_{mJ} (dominant in the depleted case) and c_{dp} (dominant in the weakly inverted case), V_{ph} ultimately increases with an inclination depending on ϕ_S.

Detectability

As mentioned so far, V_{ph} generally depends on τ_n, D_{it}, Q_f and ρ. Crystal defects, radiation damage, contamination, surface charge up and striation can thus be observed by imaging ac SPVs. From the results of the numerical analyses, minimum detectable changes in the above quantities were evaluated as shown in Table 1. For typical wafer faults, inhomogeneities in electronic characteristics throughout a wafer mostly exceed the detection limits in Table 1. In the evaluations, minimum detectable V_{ph} change was assumed to be 1%, since minimum luminance change detectable when observing a black and white TV image is considered to be about 1% (Kinameri et al, 1988).

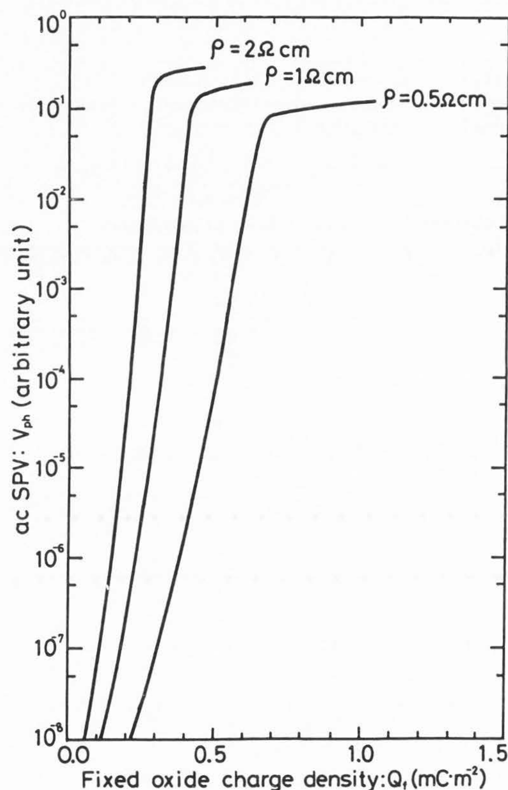

Fig. 6. Dependence of ac SPV on fixed oxide charge density.

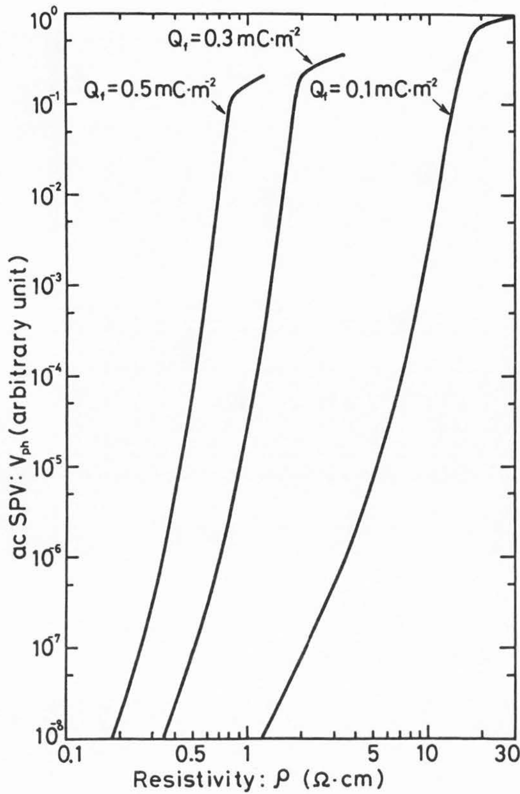

Fig. 7. Dependence of ac SPV on wafer resistivity.

Table 1. Detectabilities for ac SPV imaging[1].

	depleted	weakly inverted
τ_n	4%[2]	4%[2]
D_{it}	9%	250%[3]
Q_f	0. 07%	1%[3]
ρ	0. 1%	4%[4]

(1) changes in τ_n, D_{it}, Q_f and ρ corresponding V_{ph} change of 1% for a wafer of τ_n=10μs, ρ=1Ωcm, Q_f=0. 3mCm^{-2}, and D_{it}=10^{14}m^{-2}eV^{-1}.
(2) when excited by a 1076nm PB.
(3) when Q_f=0. 5mCm^{-2}.
(4) when ρ=3Ωcm.

Examples of Wafer Characterizations

Swirl-like Defects

Ac SPV distribution was observed for a 125mm p-type Si wafer with a thermal SiO_2 layer. An image is shown in Fig. 8a. This image was obtained using a 10μW near infrared PB. As shown, concentric ring patterns are clearly recognized.

An X-ray topograph of the same wafer is shown in Fig. 8b. It was taken using a MoK_α X-ray (55kV and 200mA electron beam irradiation) and a slit width of 1mm. Ring-like patterns similar to those in Fig. 8a are observed. These indicate swirl-like defects in the Si crystal. This proves that Fig. 8a shows the crystal defect distribution in the wafer.

The micro-defect density in the wafer was also measured by etching about 40μm from the wafer surface. It was estimated to be 2. 5×10^{7}cm^{-3} on average, and the locality (max/min) was about 3.

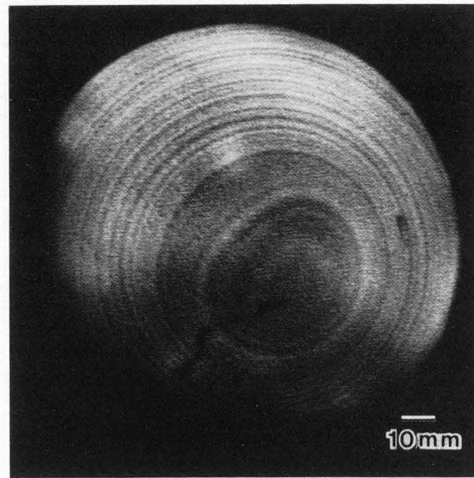

Fig. 8a. Photovoltage image for a Si wafer with swirl-like defects.

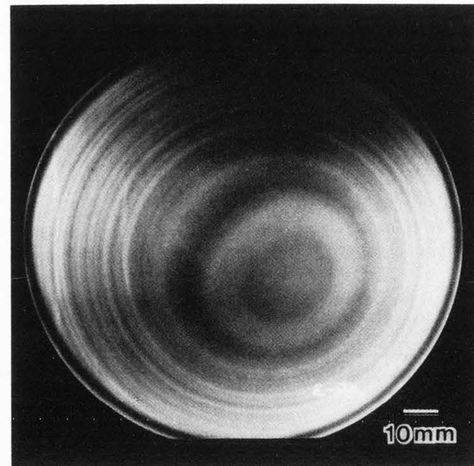

Fig. 8b. X-ray topograph for a Si wafer with Swirl-like defects.

Grain Boundaries

A near infrared PB excited ac SPV image for a 76mm polycrystalline Si solar cell, with grid electrodes at 2mm pitch, is shown in Fig. 9. The randomly curved lines in Fig. 9 are grain boundaries where minority carrier lifetime should be shorter than that in other parts because of high crystal defect density.

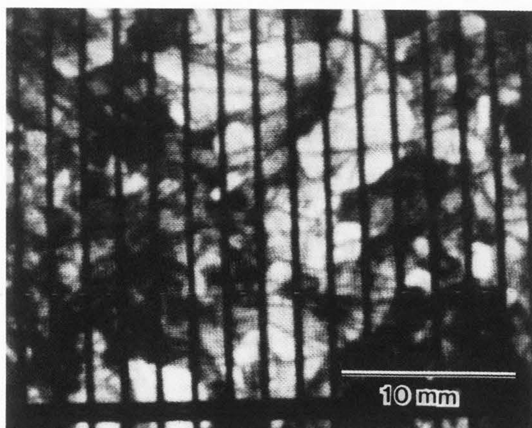

Fig. 9. Grain boundaries in a polycrystalline Si solar cell.

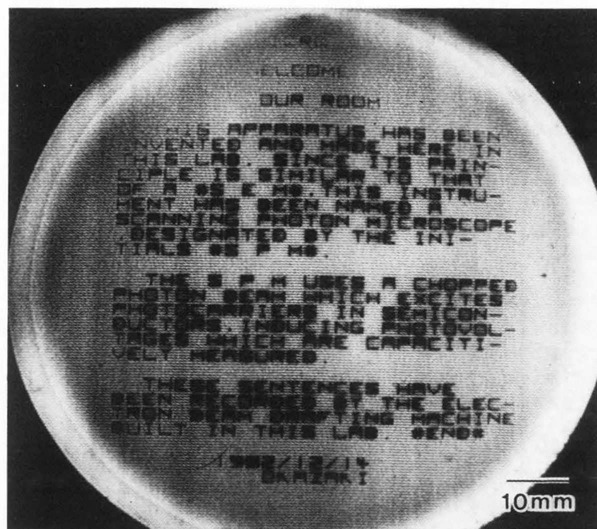

Fig. 10a. Electron beam induced radiation damage in a Si wafer observed with a 100mm×100mm viewing field.

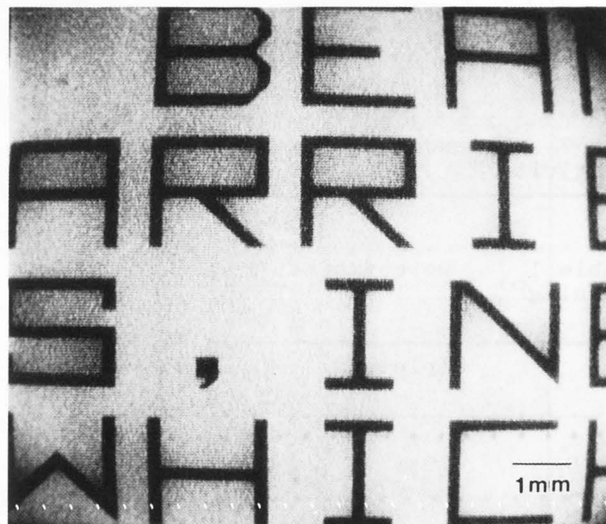

Fig. 10b. Electron beam induced radiation damage in a Si wafer observed with a 10mm×10mm viewing field.

Radiation Damage

To re-confirm the detectability of radiation damage in a Si wafer (Munakata and Miyazaki, 1981), an ac SPV image with a blue PB of about 0.4μW was obtained of a wafer in which radiation damage was intentionally induced. The specimen was a 100mm p-type Si wafer with a thermal SiO_2 layer 360nm thick and 20~40Ωcm nominal resistivity in which character patterns were recorded by an electron beam drafting machine with a dose of 30μCcm^{-2} at 30kV. The characters on the wafer were 2mm high and of 0.2mm line width. D_{it} in the electron beam (EB) damaged area was assumed to be in the order of 10^{15}m^{-2}eV^{-1}.

The observed images for a PB scanning area 100mm square is shown in Fig. 10a, while the image for a scanning area 10mm square is shown in Fig. 10b. Figure. 10b was taken by making the PB projecting magnification smaller so that the spot size on the wafer was 30μm. Since the wafer is strongly inverted in this case, ac SPV at the EB drafted characters was lower than that at the background. Ac SPV in an EB damaged area has been confirmed experimentally to be higher than that in an undamaged area in a depleted wafer (Munakata et al, 1982).

Contamination

A 100mm n-type Si wafer contaminated with sulfate ions was observed using a blue PB, as shown in Fig. 11. Since the contamination generates interface traps and the wafer is strongly inverted, ac SPV is reduced in the contaminated regions. The area at the wafer circumference with high ac SPV corresponds to an area where Mylar sheet is inserted to ensure an air gap between the wafer surface and the transparent electrode.

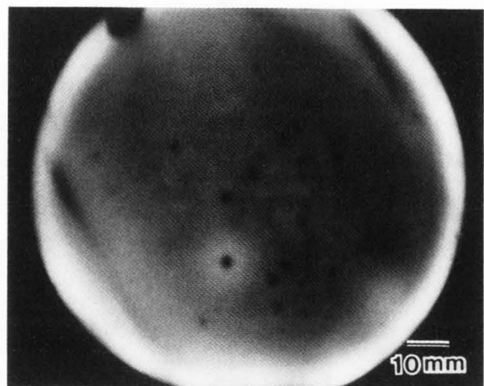

Fig. 11. Contamination due to sulfate ions.

Surface Charge-up

In semiconductor device fabrication, a photoresist layer on a wafer is usually removed by a plasma asher. This process, however, causes radiation damage including surface charge-up, since ions or electrons in the plasma are implanted into the wafer.

A blue PB excited ac SPV image for a 125mm wafer thus processed, with resistivity of 0.1Ωcm (depleted), is shown in Fig. 12. Ac SPV is assumed to rise at wafer outskirt because part of the oxide layer here is charged up additively to the fixed oxide charges. Such a charge-up pattern depends on both plasma asher equipment and wafer arrangement in the equipment.

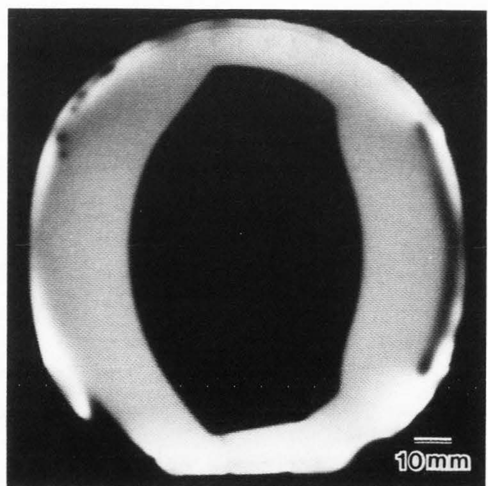

Fig. 12. Surface charge-up after plasma asher process.

Junctions in a GaAs Wafer

Ac SPV is induced even in GaAs wafers if depletion layers are formed. A near infrared PB excited ac SPV image for a 50mm semi-insulating GaAs wafer with ion implanted areas is shown in Fig. 13a. Si and Mg ions of 75keV have been implanted at $2\sim4\times10^{12}cm^{-2}$ as shown in Fig. 13b. Since the Si and Mg ion implanted areas qualify as n-type and p-type, respectively, junctions are formed at the interfaces between ion implanted layers and the semi-insulating GaAs layer. The polarities of these junctions are mutually opposite. Figures. 13c and Fig. 13d are phase discriminated ac SPV images, the discriminated phases of which are mutually opposite.

As shown, junction inhomogeneities are characterized using ac SPV images. Figure. 13a shows that very low ac SPV is induced even in areas without ion implantation. It is recognized from Fig. 13d that the phase shifts in these areas are similar to that in the Mg implanted area. This suggests that the semi-insulating GaAs surface is fairly invaded by defect trapping negative charges.

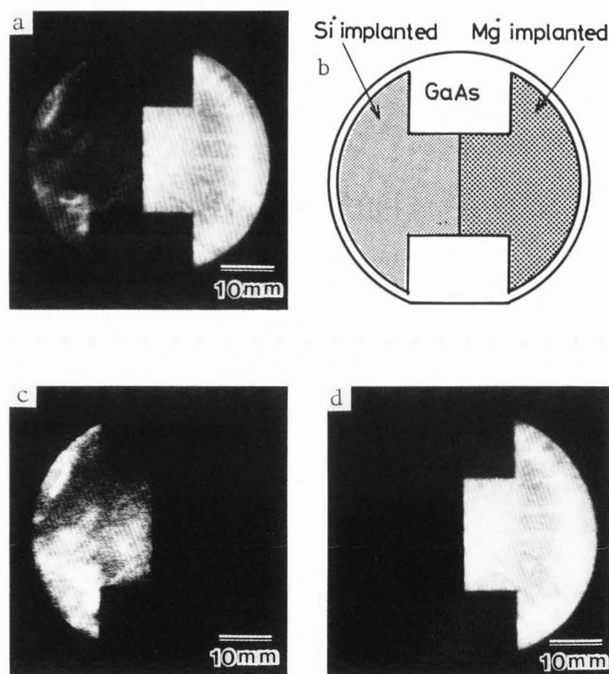

Fig. 13. Junctions in a GaAs wafer. (a)Photovoltage amplitude image, (b)ion implantation map, and (c),(d) phase discriminated photovoltage images. The discriminated phases for (c) and (d) are mutually opposite.

Conclusion

In the photovoltage imaging method, in which the distribution of ac surface photovoltages induced in a semiconductor wafer due to irradiation by a chopped photon beam is displayed as a black and white image, principles of wafer characterizations together with fault detectabilities were clarified by numerical analyses of ac surface photovoltages. This method was proven to be competent by applying it to inspections of wafer faults such as crystal defects, radiation damage, contamination and surface charge-up in Si wafers, or junction inhomogeneities in a GaAs wafer.

The development of a method and apparatus for semiconductor device characterization where high spatial resolution is required, should be a subject of future research.

Acknowledgements

The authors are grateful to Dr. Mikio Ashikawa, Mr. Koichi Mayama and Mr. Iwao Takemoto for their valuable discussion and long-term support. They also thank Dr. Hirofumi Shimizu for discussions on crystal defects and contamination. For specimen preparation and discussion, thanks are also due to Mr. Shinji Okazaki and Mr. Yoshinori Imamura who cooperated in the study on electron beam damaged wafers and ion implanted GaAs wafers, respectively.

References

Brattain WH, Garrett CGB. (1956). Combined Measurements of Field Effect, Surface Photo-voltage and Photoconductivity. *Bell Syst. Tech. J.* 35, 1019-1040.

Czaja W, Patel JR. (1965). Observations of Individual Dislocations and Oxygen Precipitates in Silicon with a Scanning Electron Beam Method. *J. Appl. Phys.* 36, 1476-1482.

de Kock AJR. (1973). Microdefects in dislocation-free silicon crystals. *Philips Res. Rep. Suppl.* No. 35, 1-105.

Haberer JR. (1967). Photoresponse Mapping of Semiconductors. *Phys. Failure in Electron.* 5, 51-82.

Iizuka T, Sugano T. (1973). Calculation of Energy Levels of Oxygen and Silicon Vacancies at the Si-SiO_2 Interface. *Jpn. J. Appl. Phys.* 12, 73-79.

Kinameri K, Munakata C, Mayama K. (1988). A scanning photon microscope for non-destructive observations of crystal defect and interface trap distributions in silicon wafers. *J. Phys. E:Sci. Instrum.* 21, 91-97.

Levy ME. (1977). An Investigation of Flaws in Complex CMOS Devices by a Scanning Photoexcitation Technique. *15th Annual Proc. Reliability Phys., Las Vegas*, 1977; (New York: IEEE Inc.); 44-53.

Mataré HF, Laakso WL. (1968). Scanning Electron Beam Display of Dislocation Space Charge. *Appl. Phys. Lett.* 13, 216-218.

Munakata C, Nanba M, Matsubara S. (1981). Non-Destructive Method of Observing Inhomogeneities in p-n Junctions with a Chopped Photon Beam. *Jpn. J. Appl. Phys.* 20, L137-L140.

Munakata C, Miyazaki M. (1981). A novel method of electron beam recording on a Si wafer. *Jpn. J. Appl. Phys.* 20, *L*293- *L*295.

Munakata C, Okazaki S, Yagi K. (1982). Electron Beam Enhanced Surface Photovoltage. *Jpn. J. Appl. Phys.* 21, *L*555-*L*557.

Munakata C, Nishimatsu S, Honma N, Yagi K. (1984). Ac Surface Photovoltages in Strongly-Inverted Oxidized p-Type Silicon Wafers. *Jpn. J. Appl. Phys.* 23, 1451-1461.

Munakata C, Nishimatsu S. (1986). Analysis of ac Surface Photovoltages in a Depleted Oxidized p-Type Silicon Wafer. *Jpn. J. Appl. Phys.* 25, 807-812.

Potter CN, Sawyer DE. (1967). Optical Scanning Techniques for Semiconductor Device Screening and Identification of Surface and Junction Phenomena. *Phys. Failure in Electron.* 5, 37-50.

Saitoh T, Warabisako T, Itoh H, Nakamura N, Tamura H, Minagawa S, Tokuyama T. (1976). Dendritic Growth of Silicon Thin Films on Alumina Ceramic and Their Application to Solar Cells. *Proc. 8th(1976) Intern. Conf., Solid State Devices, Tokyo, Jpn. J. Appl. Phys.* Suppl. 16-1 (1977), 413-416.

Wilson T, Osicki WR, Gannaway JN, Booker GR. (1979). Comparison of dislocation images obtained using the scanning optical microscope and scanning electron microscope. *J. Materials Sci.* 14, 961-965.

Wittry DB, Kyser DF. (1964). Use of Electron Probes in the Study of Recombination Radiation. *J. Appl. Phys.* 35, 2439-2442.

Discussion with Reviewers

Reviewer I: I wonder if you could compare your method with earlier approaches such as those by Goodman and DiStefano.

Authors: Our method is similar to the method by Goodman (1961) and the scanned surface photovoltage (SSP) method by Philbrick and DiStefano (1975) in the sense that surface photovoltage is capacitively measured.

In the measurement of minority carrier diffusion lengths, Goodman assumed

that the surface impedance was always neglected. In our method, surface impedance is positively used to observe interface faults such as damage and contamination.

In the SSP method, surface photovoltage is detected with a small remote electrode coupled with a conductive surface channel. Since a continuous surface channel is assumed in this method, it seems to be hard to apply the SSP method to wafers with discontinuous oxide layer patterns such as wafers at intermediate stages of device fabrication. On the other hand, our method can be applied to wafers at any stages of device fabrication because it does not require a surface channel.

R. H. Propst: Are the authors familiar with the commercially available OBIC systems and if so how does their system compare in features and resolution?
Authors: In most of commercially available scanning optical microscopes (SOMs), dc OBIC, or simply dc photocurrent, can be imaged. It is not easy to observe interface defects with OBIC mode, since the photocurrent is mainly dominated by defects in the bulk. However, our method images ac surface photovoltage which is dominated by not only the photocurrent but also by surface impedance depending on interface/surface faults such as damage, contamination and charge up. Therefore, a wide variety of wafer faults can be observed with our method compared to OBIC method.

In addition, since dc OBIC method basically requires the existence of a junction and ohmic contacts to it, the application is limited to, e.g., devices after wiring or wafers specially prepared for inspection. By contrast our method can be applied to wafers of any stages of device fabrication without any preprocessing for ohmic contacts.

The spatial resolution in our present apparatus is inferior to the commercially available SOMs, because the apparatus has been designed to observe the whole area of a large wafer in one measurement. The theoretical limit of spatial resolution will be nearly equal to that with the OBIC method, in which the resolution is mainly limited by the spot size as analyzed by Wilson and McCabe (1987).

Reviewer I: Is the photon beam really non-destructive in the sense that it does not change the electrical properties of the wafer under test? One might imagine that the beam creates hole-electron pairs in the wafer some of which could be trapped at, for example, an interface, and therefore alter / modify the interface charge density.
Authors: The changes in electrical properties due to photon beam irradiation are sufficiently small in most wafers. This may be because interface traps in those wafers are fast ones and the spot power density applied to the wafers is as low as, e.g., $10^2 Wm^{-2}$. Although photovoltages decrease after photon beam irradiation in some wafers, the photovoltages usually recover in several hours if the wafers are not irradiated. However, as you point out, it is quite possible for wafers with very slow traps that photon beam irradiation modifies the interface charge density.

R. H. Herlocher III: How stable were SPV-signals from p-type silicon after oxide growth?
Authors: The surface photovoltage (SPV) is stable for thermally oxidized silicon wafers. However, it is quite unstable for naturally oxidized silicon wafers, in which oxide layers are as thin as several nanometers. For example, the SPV in a naturally oxidized n-type wafer is very sensitive to the humidity around the specimen stage.

R. H. Herlocher III: Were images possible in the presence of an oxide on p-type silicon (and/or n-type)?
Authors: Yes, they were possible except for a thermally oxidized n-type silicon wafer. In a thermally oxidized n-type silicon wafer, surface photovoltage is very low because relatively small amount of charges are fixed in the oxide layer.

Reviewer I: Is it really the case that you need no metal contact to the wafer? It seems that you should need some form of contact to the back of the wafer to complete the circuit. You seem to show such a connection in Figure 1. What properties should such a contact, if it is indeed needed, have?
Authors: An electrical connection to the back of the wafer is not necessarily a metal (or ohmic) contact since the signal is ac voltage. A capacitive connection to the back through an air gap can also be applied as used in the wafer surface. In our present apparatus, however, a wafer is placed on a metal vacuum chuck to flatten it for the assurance of a uniform air gap at the surface. It should be noted that the connection to the back of the wafer is capacitive even in the present apparatus because the back of the wafer has usually been oxidized.

L. J. Balk: The arrangement for ac SPV detection seems to be usable for electron beam excitation, if the bottom surface of the sample is used as one of the capacitor electrodes. Do you have any experience in this respect?
Authors: Although we have not experienced the detection of ac SPV induced

by electron beam excitation, we think that such a detection is possible by using a mesh electrode instead of a transparent electrode in our apparatus.

L. J. Balk: A similar arrangement was used by Domnik et al (Detector Strategy for Highly Versatile Scanning Electron Acoustic Microscopy (SEAM), Springer Series in Optical Sciences 58 292, 1987) to generate electron acoustic (SEAM) micrographs of metals, as the capacitance changes with separation of the electrodes. Though from the experimental parameters you mention a photoacoustic contribution is very unlikely, it would have to be considered in case of high density excitations. Have you considered this?
Authors: It is presumed that a photoacoustic contribution to the detected photovoltage will be remarkable if the spot power density is extremely high, e.g., $10^7 Wm^{-2}$. However, the spot power density used in our measurement is in the order of $10^2 Wm^{-2}$. In such low density excitation, the photoacoustic contribution will be sufficiently small.

Reviewer I: Does the speed at which you scan the photon beam play any part in the SPV image formation other than providing a very convenient real time image?
Authors: In this method, a lock-in amplifier is used to amplify ac photovoltage because the detected photovoltage is as low as, e.g., microvolts. Therefore, the measurement speed is restricted by the time constant of the lock-in amplifier, which is 1ms for the present apparatus.

R. H. Propst: You need to show external circuit to make clear how the photovoltage (really photocurrent is I-V converted?) generates the signal on CRT.
Authors: We intended to emphasize the most essential part of the apparatus in Fig. 1, especially the configuration of the photovoltage detector. The detailed construction of over-all system including external circuit has already been shown in our previous paper ("text reference", Kinameri et al, 1988).

R. H. Propst: How did you calculate ac surface photovoltage? How do interface trap density, fixed oxide charge density and resistivity dominate the surface impedance?
Authors: The procedures and equations for calculating ac surface photovoltages have been shown in the previous paper by one of the authors ("text reference", Munakata et al, 1984, and Munakata and Nishimatsu, 1986). The curves shown in Figs. 4, 5, 6 and 7 are the results of numerical calculations which exactly follow these procedures and equations. In these equations, the surface impedance is expressed as a function of interface trap density, fixed oxide charge density and resistivity.

R. H. Propst: What is your minimum threshold of radiation damage detection?
Authors: Interface trap density, D_{it}, would be one of measures to evaluate the degree of radiation damage. In our experiences, D_{it} for a normal wafer is considered to be approximately $1\times10^{14} eV^{-1}m^{-2}$. According to our numerical analysis of ac surface photovoltage dependence on D_{it}, photovoltage decreases by 1% when D_{it} increases by 3.5 times in a weakly inverted wafer. Thus, radiation damage corresponding to D_{it} of $3.5\times10^{14} eV^{-1}m^{-2}$ can be detected with this method.

Additional References

Goodman AM. (1961). A method for the Measurement of Short Minority Carrier Diffusion lengths in Semiconductors. *J. Appl. Phys.* 32, 2550-2552.

Philbrick JN, DiStefano TH. (1975). Scanned surface photovoltage detection of defects in silicon wafers. *13th Annual Proc. Reliability Phys., Las Vegas* (New York: IEEE) pp159-167.

Wilson T, McCabe EM. (1987). Theory of optical beam induced current images of defects in semiconductors. *J. Appl. Phys.* 61, 191-195.